Modifying Ionogel Solid-Electrolytes for Complex Electrochemical Systems

David S Ashby^l,*, Jorge Cardenas², Austin Suhas Bhandarkar^l, Adam W. Cook², & A. Alec Talin^l,*

¹Sandia National Laboratories, Livermore, California 94550, USA

²Sandia National Laboratories, Albuquerque, New Mexico 87123, USA

Keywords: Ionogels, Li-ion batteries, custom architectures, solvent exchange, electrolyte

ABSTRACT

The solution processability of ionogel solid electrolytes have recently garnered interest in the Li-ion battery community as a means to address the interface and fabrication issues commonly associated with most solid-electrolytes. However, the trapped ionic liquid (ILE) component has hindered the electrochemical performance. Herein, we present a process to tune the properties by replacing the ILE in a silica-based ionogel after fabrication with a liquid component befitting the desired application. Electrochemical cycling under various conditions showcases gels containing different liquid components incorporated into LiFePO₄ (LFP)/gel/Li cells: high power (455 W kg⁻¹ at a 1C discharge) systems using carbonates, low temperature (-40 °C) using ethers, or high temperature (100 °C) using ionic liquids. Fabrication of additive manufactured (AM) cells utilizing the exchanged carbonate-based system is demonstrated in a planar LFP/Li₄Ti₅O₁₂ (LTO) system, where a marked improvement over an ionogel is found in terms of rate capability, capacity, and cycle stability (118 vs 41 mAh g⁻¹ at C/4). This process represents a promising route to create a separatorless cell, potentially in complex architectures, where the electrolyte properties can be facilely tuned to meet the required conditions for a wide range of battery chemistries while maintaining uniform electrolyte access throughout cast electrodes.

INTRODUCTION

Demand for mobile electronics, electric vehicles, and renewable energy technologies has substantially increased the requirements placed on energy storage systems, specifically Li-ion batteries (LIBs), in terms of energy and power density, reliability, and safety. With the advent of several solid-state electrolytes (SSE) that have ionic conductivities on par with liquid organic electrolytes, solid-state Li-ion batteries (SSLBs) have attracted significant attention in industry and academia as a leading solution to address the safety and reliability challenges attributed to liquid LIB electrolytes, while maintaining comparable energy and power densities. Unfortunately, substantial improvements to SSLB performance are still needed for widespread commercialization, such as addressing fabrication issues related to poor SSE incorporation into cast electrodes and addressing high interfacial resistances, stemming primarily from interfacial reactions and lack of intimate contact.²

Ionogels (IG), a class of solid-electrolytes, have recently garnered interest due to their ability to be processed as a liquid, ensuring formation of a uniform, low resistance electrode/electrolyte interface throughout a cast electrode. Composed of ionic liquid electrolyte (ILE) trapped inside a solid nanoporous matrix, these systems nanoscopically behave like the trapped liquid, while macroscopically, they exhibit the mechanical and dimensional stability of the matrix material. Typically, these structures are formed by creating a homogeneous solution composed of electrolyte and matrix precursor, such as a dissolved

^{*}Correspondence: dsashby18@gmail.com, aatalin@sandia.gov

polymer or alkoxide-derived inorganic sol. Upon processing and solidification, the electrolyte becomes trapped within the network. For oxide-based ionogels, these systems can be considered as nano-sponges, where a high degree of interconnected nanopores provide facile transport and produce sufficient capillary force to entrap the liquid, similar to other confinement electrolytes such as metal-organic and covalent-organic frameworks (MOFs and COFs)^{3–5} and polymer systems⁶. The initial liquid state permits multiple processing routes to obtain uniform depositions, such as spin coating⁷, ink-jet printing⁸, or dip coating⁹.

The solution-processability of ionogels is an attractive feature for integration into complex architectures or high-weight-loading cells. However, the use of low vapor-pressure ionic liquids, required for processing, ¹⁰ severely limits their use in LIBs. While ionic liquids have several beneficial properties, such as a high thermal and electrochemical stability, their low ionic conductivity, low Li⁺ transference number, and typical poor low-temperature performance limit the potential application space to low power systems. ^{11,12} Further, electrochemical instability with low voltage anodes ¹³, such as Li metal or Si, limits the maximum achievable energy density. Due to these and other limitations such as cost, ionogels have not been readily adopted commercially.

Herein, we present a process whereby the ionic liquid trapped inside a nanoporous matrix is replaced with an alternative liquid electrolyte, thus demonstrating a SSLB system with highly tunable physicochemical and interfacial properties. Exchange occurs after sol incorporation into a composite electrode and solidification has occurred to ensure uniform electrode wetting and a low interfacial resistance is maintained. In this study, a spin-coated, SiO₂ ionogel is exchanged with several different electrolytes to assess the degree of exchange and the effect on the cell performance. We demonstrate complete ILE (1M LiFSI PYR₁₄TFSI) exchange for 1M LiFSI DOL/DME and 1M LiClO₄ PC as verified using Raman spectroscopy and thermal gravimetric analysis (TGA). Using cells composed of LiFePO₄ (LFP)/exchanged gels/Li, we demonstrate improved low temperature performance for the DOL/DME-based electrolyte and high-power performance for the carbonate-based electrolyte compared to similar cells with ionic-liquid-based ionogels. These cells have similar performance to the corresponding liquid electrolyte composed cells. In addition, we demonstrate our novel exchange process in additive manufactured (AM) cells composed of LFP/gel/LTO. The cycling of both the cast and AM cells indicate that neither process has a detrimental effect on the solid matrix and entrapment does not undesirably impact the electrochemical properties of the newly confined liquid, permitting design freedom for both composition and architecture.

RESULTS

Fabrication of a solvent-exchanged gel from a silica-based ionogel was conducted through a multistep process. First, ionogels, modifying a previously reported process, were spun onto LFP cast electrodes to an approximate thickness of 10 microns (Figure S1) or drop cast into bulk molds for analysis. The ionogel was allowed to age overnight before drying in a vacuum oven to remove any residual alcohol or water produced during the sol-gel process. Exchange occurred in an Ar glovebox through a multi-step process, where the electrodes were soaked for two or more hours in an excess of the parent electrolyte. This was repeated three times with new electrolyte to ensure complete exchange (Figure 1a). PC and DOL/DME based electrolytes were chosen for exchange to represent carbonate and ether-based electrolytes were chosen for exchange to represent carbonate and ether-based electrolytes has a low solubility with the ionic liquid. While not required here, in systems where the electrolyte has a low solubility with the ionic liquid, an intermediate solvent could be used to facilitate the exchange.

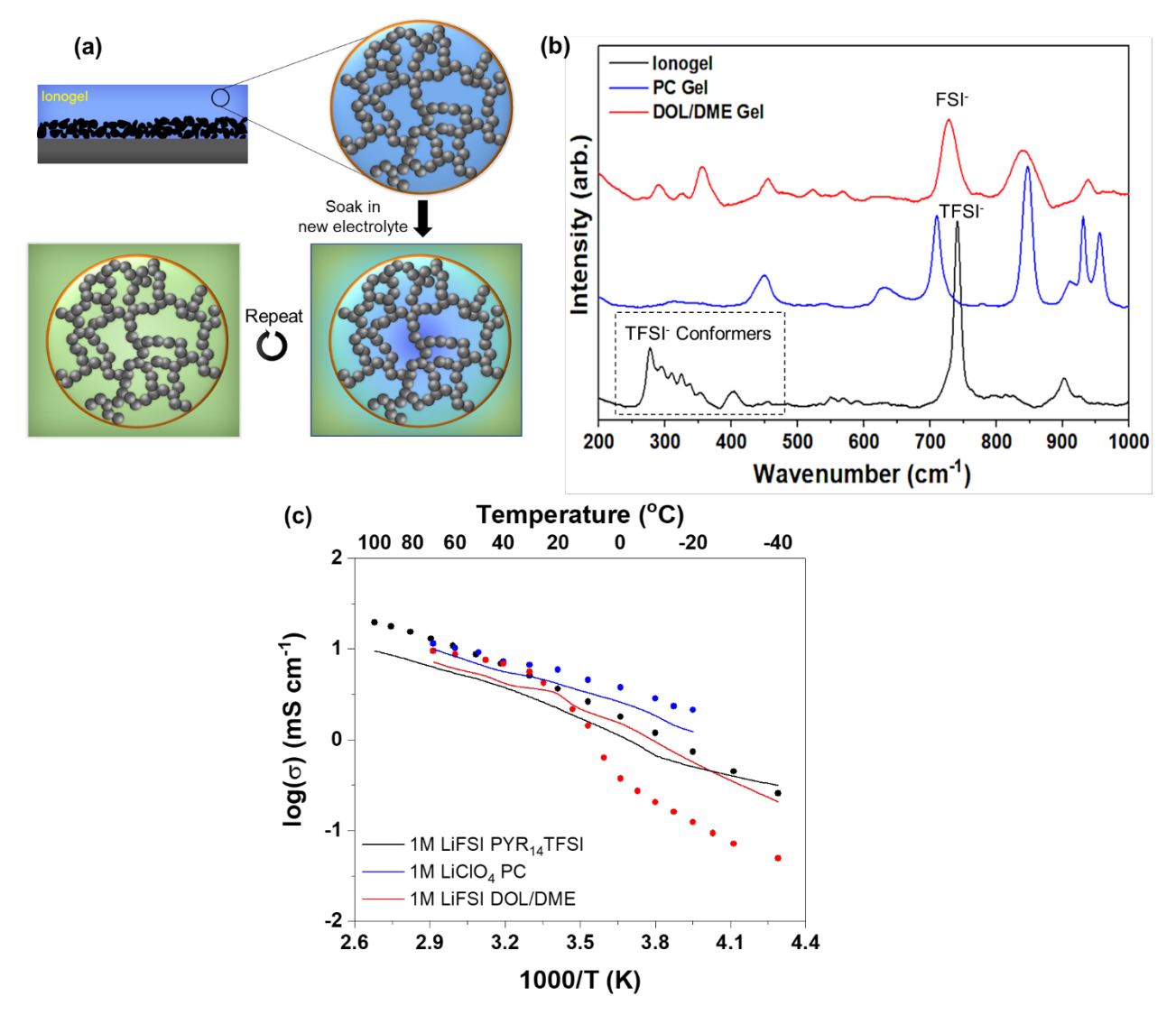


Figure 1. Physicochemical properties of Solvent-Exchanged Gels

a) Solvent exchange process schematic where the trapped ionic liquid is replaced with a new electrolyte. b) Raman spectroscopy of the ILE (black), PC (blue) and DOL/DME (red) gels. The TFSI peaks are labeled as indicators of the ILE. c) Ionic conductivity versus temperature for the gel electrolytes (line) and corresponding liquids (circles).

To determine the extent of solvent exchange, the physicochemical properties of the bulk gels after exchange were compared to the base ionogel and neat liquid electrolytes. Raman analysis of the exchange gels indicate all peaks associated with the TFSI anion disappear, signifying that the ionic liquid has been successfully replaced inside the silica structure (**Figure 1b**). A new peak associated with the DOL ring opening is identified at approximately 850 cm⁻¹ for the ether system. All other peaks in the DOL/DME and PC spectra can be assigned to the expected signature for the corresponding exchanged solvent and lithium salt.^{18–20} It is unclear whether the ring opening originates from the use of LiFSI or if the silica matrix catalyzes the reaction.^{21,22} To support that exchange was complete, as indicated by the Raman data, TGA of the base electrolyte and exchanged gels was performed (**Figure S2**). The TGA results show no weight loss attributed to the PYR₁₄TFSI ionic liquid (~400 °C)²³; only weight loss associated with the PC (~180 °C)²⁴ and DOL/DME (~100 °C)²⁵ components is identified. The remaining weight is primarily associated to the silica matrix, with the silica content falling within the expected range for the fabrication process. A shift in

the corresponding decomposition temperatures to higher values is identified for both the DOL/DME and PC gels as confinement by the silica matrix inhibits breakdown, similar to previous studies of confined liquids.²⁶ To assess whether the exchange impacts the matrix structure, the bulk gels were super-critically dried to suppress the silica skeleton collapse, followed by porosity analysis using N₂ gas adsorption (**Figure S3**). Brunauer–Emmett–Teller (BET) analysis of the gas isotherms demonstrates that the exchanged gels maintain a high surface area of at least 700 m² g⁻¹. As gelation is complete before exchange, the exchanged matrix maintains the pore distribution of the original gel, with the pore size determined by the initial ILE stacking (Figure S3b).²⁷ Variations in the surface area between the ionogel and exchanged gels likely stems from incomplete solvent removal during drying which led to pore collapse. Measurement of the ionic conductivity for the various systems indicates comparable conductivities and activation energies between the free electrolyte and gel-based systems (Figure 1c). The slightly lower conductivities for the gels follows previous studies that indicated the silica matrix increases the ion path tortuosity and decreases the total liquid volume. 28 The relative lower conductivity of the DOL/DME gel can be explained by the polymerization of DOL. ^{29–31} All conductivities of the free electrolytes agree well with reported values in literature.

After establishing that solvent exchange was successful, the electrochemical performance of LFP/Li metal cells containing the various gels was compared against each other and to the corresponding liquid systems. When comparing the liquid electrolyte cells (Figure 2a), a high cycle stability is found for all three electrolytes (~0.15% loss per cycle). As expected, the best rate capability is found for the PC electrolyte as the higher viscosity and/or lower lithium transference number of the DOL/DME and ILE electrolytes hinders ion conduction, lowering the system conductivity (Figure 1c). At lower currents, a worse columbic efficiency is identified, for the ILE cell, not seen for other electrolytes, which likely stems from the ILE instability with lithium metal. 13 Depending on the trapped electrolyte, the performance of the gels can vary widely (Figure 2b). For the ionogel, a significant decrease in the rate capability is identified (Figure S4a). This likely stems from the ionic liquid interaction with charged species on the silica wall^{32,33}, essentially narrowing the pore for Li⁺ transport. A similar decrease in the rate capability has been identified in other silica-based ionogel systems. However, comparing the PC gel to the neat liquid, an almost identical electrochemical response is identified (Figure S4b), indicating the silica matrix does not significantly hinder lithium transport in the carbonate-based system. The DOL/DME system shows similar results as the liquid, though a significant decrease in the cycle stability at 1C occurs that is not seen in the liquid system (Figure S4c). This instability could stem from the identified poly-DOL species that may hinder Li⁺ movement at higher rates by obstructing the structure, making it inaccessible to further Li⁺ transport. This could explain the increased capacity loss seen even after reducing the current. The electrochemical performance of the different gels correlates well to the initial polarization and cell impedance, where the gel resistance decreases as the liquid component transitions from ILE to DOL/DME or PC (Figure 2c, S5). This decrease in the gel resistance follows the measured conductivity trend and correlates to the expected solvents interaction with the silica matrix walls, as determined by the degree of hydrogen bonding.^{34,35} Similar to ionogels,^{7,36} we expect many of the exchanged systems fundamental characteristics, such as the Li⁺ transference number, electrochemical stabilility window, and SEI products, to be the same as the base liquid systems. Further study is required into the impact entrappment in the silica matrix has on the formation and growth of Li dendrites for these systems.

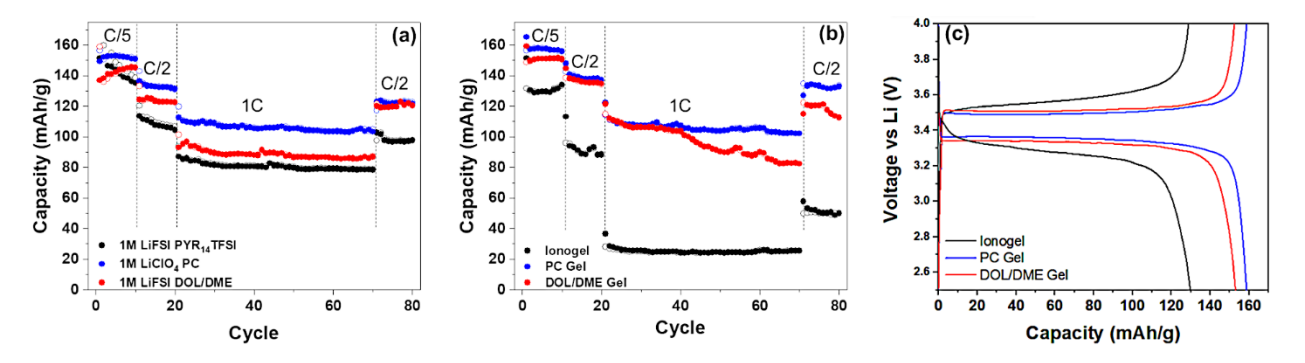


Figure 2. Room-temperature, Electrochemical Performance of Solvent-Exchanged Gels a) Charge (solid) and discharge (open) capacity variation with cycling at varying C rates for the ILE, PC, and DOL/DME liquid electrolytes. The performance corresponds well to the electrolyte ionic conductivity trend. b) Capacity variation with cycling at varying C rates for the ILE, PC, and DOL/DME gel electrolytes. No hindrance by the silica matrix, identified in the DOL/DME and ionogel cycling, is found for the carbonate-based gel. c) 2nd galvanostatic cycle at C/5 for the ILE, PC, and DOL/DME gel electrolytes.

To further illustrate the advantages of our solvent exchange process, the electrochemical performance was evaluated at different temperatures and in AM architectures. High temperature (100°C) in a LFP/Ionogel/Li cell was explored first to showcase the stability of the base silica matrix to extreme environment and high rate conditions. The ionogel ws chosen to demonstrate this due to its high thermal and electrochemical stability³⁷, which aligns well to high temperature applications. ^{38,39} Typically, these temperatures are unobtainable for most liquid or polymer electrolytes due to the safety hazards associated with solvent flammability. 40 By increasing the temperature, the electrolytic and charge transfer resistance notably decreases (Figure 3a), which enables achievement of stable capacities over 160 mAh g⁻¹ at 1C, six-times higher than the room temperature performance (**Figure 3b**). Further, use of the ionogel improved the columbic efficiency of the cell, in comparison to the liquid cell at 100°C (Figures S6 and S7), likely by suppressing adverse reactions at the lithium anode. While able to be cycled to high temperatures, the propensity for ionic liquids to solidify at temperatures close to 0 °C make them incompatible for many low temperature applications (Figure S8).⁴¹ As such, the DOL/DME system, which has shown some success at low temperatures 42, was explored at -40 °C to evaluate the low temperature performance of an exchanged gel. Figure 3c demonstrates reasonable capacities (95 mAh g⁻¹) for the DOL/DME systems at low rates (C/20), with similar performance maintained between the gel and liquid cycled at higher currents (~60 mAh g⁻¹ at C/5, **Figure 3d**). The multiple, identifiable plateaus in the liquid DOL/DME system likely stem from the electrolyte being frozen to different degrees. While the DOL/DME system has not been optimized for low temperature applications, 42,43 it still demonstrates adequate performance especially when incorporated into the silica matrix. Further low-temperature improvement could be achieved through use of designer electrolytes, such as the all-fluorinated systems, 44 which should be facilely incorporated into the silica matrix due to the affinity of fluorine to silica⁴⁵.

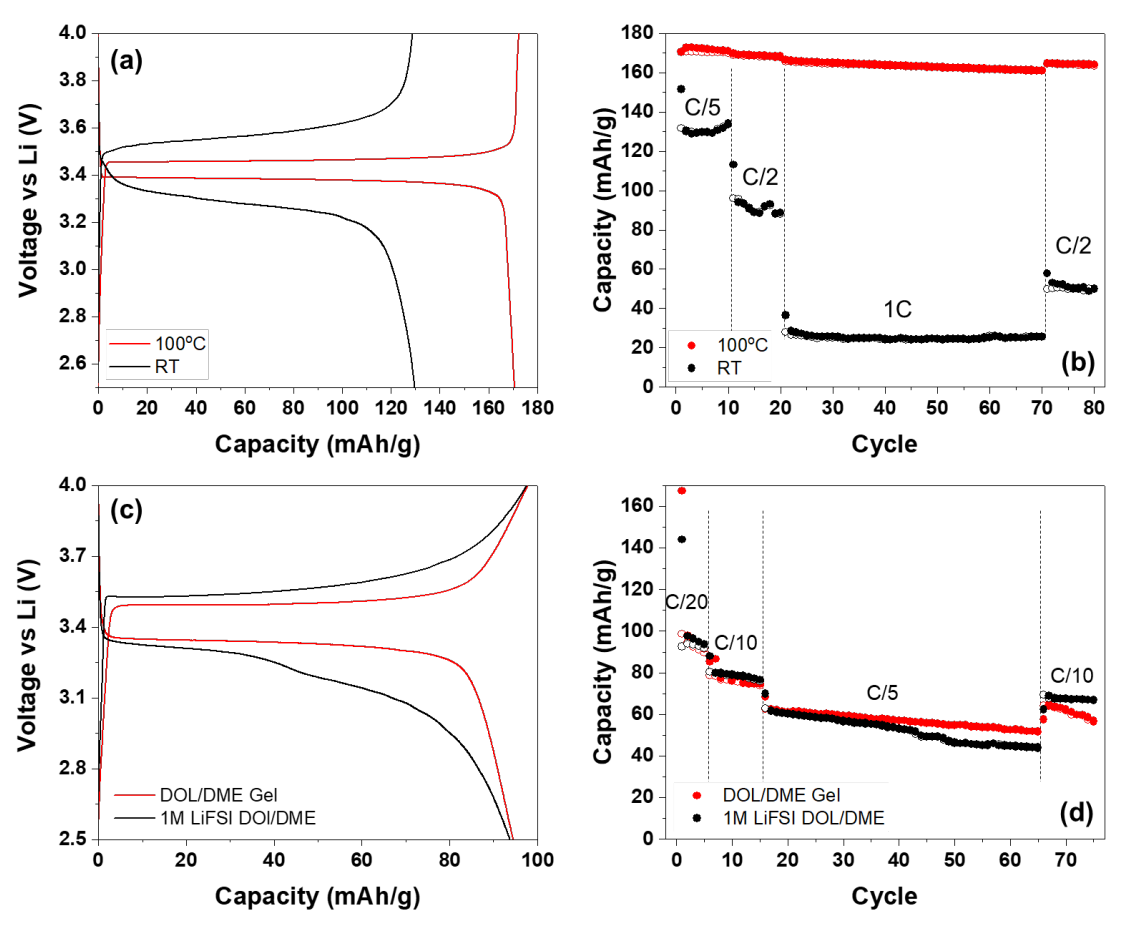


Figure 3. Electrochemical Performance at Varying Temperatures a) 2nd galvanostatic cycle at C/5 for the ionogel electrolyte cycled at room temperature (RT, black) and 100 °C (red). b) Charge (solid) and discharge (open) capacity variation with cycling at varying C rates for the ionogel system at temperature. The improved performance at 100 °C corresponds well to decreased polarization identified in the galvanostatic (a) and EIS data (**Figure S9**). c) 2nd galvanostatic cycle at C/20 for the DOL/DME liquid (black) and gel (red) systems cycled at -40 °C. d) Charge (solid) and discharge (open) capacity variation with cycling at varying C rates for the DOL/DME systems at -40 °C.

In addition to its potential utility in traditional cast cells, the novelty of the electrolyte exchange is best exemplified in additively manufactured (AM) systems that cannot be readily fabricated with current solid electrolyte processes. To this end, a cell made using direct-inkwrite printing (Figure 4a), composed of an LFP/Ionogel/LTO AM stack, was exchanged with the 1M LiClO₄ PC electrolyte and compared to the ionogel. An exemplary image of AM process of the IG electrolyte over a large area is shown in Figure 4b. Exploring the electrochemical performance, Figure 4c demonstrates that while reasonable capacities can be achieved for the carbonate gel (118 mAh g⁻¹ at C/4), the ionogel system is severely limited (41 mAh g⁻¹ at C/4) due to its low conduction and transference number. As with the cast electrodes, similar behavior is maintained between the base PC liquid and PC gel at lower rates while the ionogel behaved significantly worse than the base ILE. The difference in the initial capacity between the gel and liquid systems likely stems from varying accessibility to the active material originiating from the AM process. The loss of capacity over the extended cycling and lower capacity at higher rates for the gels in comparison to the base liquids likely stems from heterogeneity in the gel introduced by the unoptimized AM process. While the gels have a higher impedance than the base liquids (Figure S10), the performance of the

different AM cells correlate closer to the polarization displayed in the GVs (**Figure 4d**). The complete AM fabrication presents a route to create unique architectural and composition solid-state cells that are impractical with current methods while maintaining the properties dictated by the exchanged electrolyte. Noteworthy of ionogels, by controlling the assembly process, the preliminary solid electrolytes can be uniformly incorporated throughout each AM electrode before joining of the full cell, ensuring uniform access.

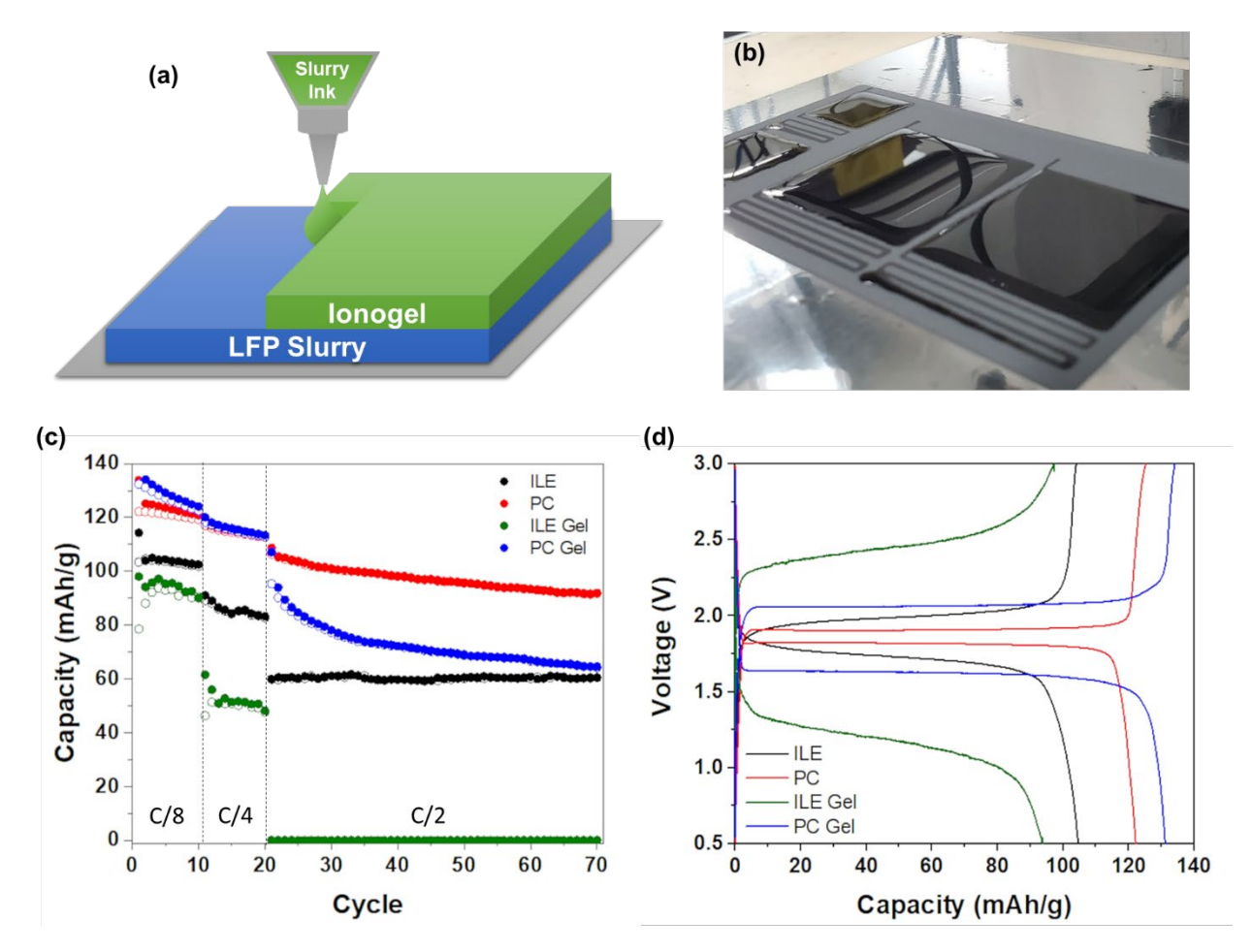


Figure 4. Electrochemical Performance of Additive Manufactured Cells a) Schematic of the AM printing process. The laminated electrode is manufactured in a two-step direct writing process: first printing of the electrode slurry before printing the ionogel on the dried electrode. b) Exemplary image of AM printed large area ionogel electrolyte films onto LFP cathode with aluminum foil substrate. c) Charge (solid) and discharge (open) capacity variation with cycling at varying C rates for AM LFP/LTO cells using ILE, PC, ILE gel, or PC gel electrolyte. d) 2nd galvanostatic cycle at C/8 for AM LFP/LTO cells cycled using ILE, PC, ILE gel, or PC gel electrolyte.

DISCUSSION

The ability to exchange electrolytes into a solution-processable, pseudo-solid electrolyte exemplified here offers a unique solution to address fabrication or performance issues typically associated with ionogels or solid-electrolytes, while providing an opportunity to tailor the electrolyte properties to suit the application. Though the exchange process increases the fabrication cost and time, it provides an innovative way to create an electrolyte for custom applications that traditionally has been challenging, such as the complex architectures or extreme conditions required by the aerospace industry⁴⁶. From a fundamental

standpoint, the process provides an opportunity to investigate the interaction of the same porous matrix with different electrolytes and potentially design systems with emergent behaviors. Our system differs from the previous studies conducted using MOFs or COFs in that the matrix represents a scalable, manufacturable process that can be facily modifed to control the pore structure. 11,47 This technique's novelty is best demonstrated by the representative AM cell. The use of an AM process allows the creation of complex designed cells where the incorporation with most solid electrolytes is infeasible. Due to the flexibility of the additive manufacturing and utilizing the functionality of the solvent exchange processes, many other custom shapes can be realized that could not be achieved using conventional liquid electrolytes and separators. Multidimensional batteries, an approach to improve volumetric and areal energy and power, represent one such area of interest as the electrolyte's fabrication process and performance has traditionally been the limiting factors. By replacing traditionally used electrolytes for the PC-exchanged gel, the high aspect ratio structures would be able to overcome the lithiation starvation near the base that currently limit these and like systems. 48 Though only the DOL/DME and PC systems were demonstrated in this study, we believe that this process is ubiquitous for most commonly used electrolytes due to the high solubility of most organic solvents in ionic liquids¹⁷ and due to the silica matrix's mechanical and chemical stability.⁴⁹ The pyrrolidinium system was used here for comparison of the electrochemical performance, but more feasible scaling could be achieved by replacing it with a cheaper, less viscous, aprotic ionic liquid. Similarly, while LFP and LTO were used as exemplar electrode materials, ionogels have been demonstrated to be stable or modifiable for a range of different lithium chemistries. ^{36,50} The solvent-exchange approach presented here for improving ionogel electrolytes represents a facile method to tailor the electrochemical properties of a solution-processable solid electrolyte. This enables improved compatibility and performance for a wide range of chemistries, environmental conditions, and geometries. While limited here to LIBs, our approach presents a novel platform with implications beyond LIBs, such as for neuromorphic computing⁵¹, other ion electrochemicalstorage-systems⁵², or fundamental analysis of electrolyte confinement effects⁵³.

CONCLUSION

While solid electrolytes have demonstrated promising performance under standard conditions, processing issues and poor wetting has significantly limited their potential usage in comparison to their liquid counterparts. Due to the limitations imposed by the trapped ionic liquid to the ionogel electrochemical performance, modification of a silica-based system is explored through a solvent exchange process to tune the electrolytic properties as means to suit the application. Here, we demonstrate the ability to achieve a solution-processable, solid electrolyte that has been facilely modified for high power applications through a carbonate electrolyte, low temperature performance through DOL/DME, or high temperature applications by maintaining the base ILE. Solvent exchange is further demonstrated in a complex architecture, unobtainable with most solid-electrolyte processing techniques. This solvent exchange process demonstrates a unique way to tailor a pseudo-solid electrolyte properties to meet the desired application requirements, whether they be constrained by environmental, power, or geometrical limitations. By further incorporating this process into newer fabrication techniques, such as additive manufacturing, improved performance can be obtained in currently infeasible architectures and geometries.

EXPERIMENTAL METHODS

Electrode Formulation:

LiFePO₄ (LFP, Skyspring Nanomaterials), lithium titanate (LTO, Sigma Aldrich), lithium foil (Sigma Aldrich), reduced graphene oxide (rGO, Graphenea), Super P carbon black (Timcal), polyvinylidene fluoride (PVDF, Kynar HSV900), and n-methyl-2-pyrrolidone (NMP, Sigma Aldrich anhydrous) were used without further processing. The cathode slurry, consisting of 80 wt% LFP, 5 wt% rGO, 5 wt% Super P, and 10 wt% PVDF, was suspended in NMP before casting onto carbon-coated aluminum foil to an approximate loading of 3 mg cm⁻² and thickness of 50 μm. All electrodes were dried in a 150 °C vacuum oven and calendered under a linear press at 5 tons before assembly.

Tetraethylorthosilicate (TEOS, >99%, Sigma Aldrich), triethylvinylorthosilicate (VTEOS,

Ionogel Synthesis and Fabrication:

97%, Sigma Aldrich), and formic acid (Puram, Fluka Analytical) were used for the silica solgel reaction. The ionic liquid electrolyte was produced from lithium bis(fluoromethanesulfonyl)imide (LiFSI, Sigma Aldrich) and 1-butyl-1-methylpyrrolidinium bis(trifluoromethylsulfonyl)imide (PYR₁₄ TFSI, 99.5%, Solvionic). Ionic liquid was first degassed using a vacuum oven before storing inside an Ar-gas-filled glovebox (l ppm H₂O). 1M LiFSI PYR₁₄ TFSI ionic liquid electrolyte (ILE) was then prepared from the degassed ionic liquid. The sol was composed of equal volumetric ratios of the silica precursors and acid catalyst. The sol was mixed with the ILE in a 60:40 volumetric ratio. Two different gels were formed for electrochemical analysis. The sol was either spun directly onto the electrodes (solution processed) or allowed to gel and dry in a polypropylene mold before being extracted for bulk testing. The films were spun twice at 1500 rpm (CEE Apogee coater) with an hour rest in between spins to achieve a uniform coating across the electrode. Gelation took approximately 2 hours for the spun films and overnight for the bulk gels. The gelation times were sufficiently long to ensure uniform sol penetration into the electrode.

Solvent-exchange Process:

Anhyhdrous lithium perchlorate (LiClO₄, Sigma Aldrich), lithium bis(fluoromethanesulfonyl)imide (LiFSI, Sigma Aldrich), propylene carbonate (PC, Sigma Aldrich), 1,3 dioxolane (DOL, Sigma Aldrich), and dimethyl ether (DME, Sigma Aldrich) were obtained for the synthesis of 1M LiClO₄ PC and 1M LiFSI DOL/DME (1:1 vol) electrolytes for solvent exchange.

Bulk or spun ionogels were exchanged with the PC or DOL/DME electrolytes through a multistep process. To exchange, the gels were soaked in excess PC or DOL/DME electrolyte for a minimum of 2 hours. This was repeated three times total, each time in clean electrolyte, to ensure complete exchange. All exchange and sample preparations were performed inside an Ar glovebox. As DOL/DME and PC are soluble with the ionic liquid, no intermediate solvent was required.

Physicochemical Analysis:

Raman analysis (Renishaw inVia confocal Raman microscope) was performed on the bulk exchanged gels. The analysis was performed with a 532 nm Ar laser and 1800/mm grating through a 20× objective lens. Thermal gravimetric analysis (TGA, TA Instruments) on the Raman-studied gels was performed from 30-550 °C at 5°K min⁻¹ under air flow. Analysis was performed in an aluminum pan.

N₂ adsorption testing was performed using a Micromeritics ASAP 2020 instrument. To characterize the silica network in the ionogel, we modified a procedure reported previously.⁵⁴ In the current case, the gels were immersed in ethanol to replace the trapped liquid. Then, the ethanol is removed by supercritical drying using liquid CO₂ in a Tousimis Samdri Dryer. In this way, the alcohol is removed without generating the capillary forces that would collapse

the SiO_2 network. Samples were outgassed overnight at 110 °C before testing. Testing was conducted at 77° K. Brunauer–Emmett–Teller (BET) surface areas were calculated at 0.2 P/Po and the pore distribution was calculated using Micromeritics Tarazona DFT adsorption model from the isotherm data.

Conductivity data was collected from electrochemical impedance spectroscopy (EIS) measurements made using a BioLogic SP300 potentiostat on the gels and liquids that were sandwiched between stainless steel rods at temperatures between -40 to 100 °C. The frequency range for the EIS was from 1 MHz to 1 Hz with a 10mV amplitude.

Additive Manufactured Custom Architectures:

LFP, LTO, and ILE gel solutions were digitally patterned using a custom-built direct ink write (DIW) printer. Solutions were placed into 10 mL syringes and extruded through 250 μm nozzles to print thin films on planar and non-planer surfaces. The volumetric rate of material extrusion was 0.375 uL s⁻¹, 0.540 uL s⁻¹, and 0.589 uL s⁻¹ for LFP, LTO and ionogel, respectively and the printing speed was fixed at 10 mm s⁻¹. A constant nozzle offset of 150 μm from the surface of the substrate was maintained during deposition. LFP (3 mg/cm²) and LTO (3.3 mg/cm²) films were printed on aluminum foil by rastering the nozzle's toolpath such that continuous rectangular films were produced. Prior to placing ILE gels in syringe, the solution was aged at 80 °C for 3 hours on a hot plate to partially polymerize the solution and slightly increase its viscosity. This step promoted printed films shape retention as required for subsequent handling. A supplementary video of the ILE gel printing process can be found in Supplementary Video 1. These aged ILE gels were printed directly onto LFP and LTO films and punched prior to full gel polymerization to prevent cracking.

Electrochemical Analysis:

Galvanostatic, two electrode cycling using a Biologic SP300 potentiostat was performed in a CR2032 coin using the ionogel, PC, or DOL/DME systems as electrolyte. Glass fiber separators (Whatman GF/C) were used as required with 100 μL of the corresponding electrolyte being tested. 700 μm Li foils (Sigma) were used as the counter electrode with 300x excess capacity to minimize any limitations due to SEI formation. The LTO loading was controlled to give a NP ratio of 1.1 at C/8. The applied current density range was dependent on the temperature being studied. Room temperature varied between 21-23°C. Cycling was performed between 2.5-4V for the LFP/Li cell or 0.5-3V for the LFP/LTO cell. EIS data was collected before each cycle from 1MHz to 100mHz at a 10mV amplitude. The energy was calculated by integrating the voltage versus capacity curve at each cycle rate with the power being derived from the actual cycle time and energy.

SUPORTING INFORMATION

Spun Ionogel, Thermal Gravimetric Analysis of Solvent-Exchanged Gels, Gas Adsorption of Exchanged Gels, Electrochemical Comparison of Gel, Electrochemical Performance at Temperatures, EIS Analysis of Solvent-Exchanged Gels, Low Temperature Performance, EIS of Ionogel with Temperature, EIS of the AM LFP/LTO Cells, ILE Gel Printing Process

AUTHOR INFORMATION

dsashby@sandia.gov, aatalin@sandia.gov

The authors declare no competing financial interest.

ACKNOWLEDGEMENTS

The work at Sandia National Laboratories was supported by the Laboratory-Directed Research and Development (LDRD) Programs. Sandia National Laboratories is a multimission laboratory managed and operated by National Technology and Engineering Solutions of Sandia, LLC, a wholly owned subsidiary of Honeywell International Inc., for the U.S. Department of Energy's National Nuclear Security Administration under contract DE-NA-0003525. This paper describes objective technical results and analysis. Any subjective views or opinions that might be expressed in the paper do not necessarily represent the views of the U.S. Department of Energy or the United States Government.

References

- (1) Lau, J.; DeBlock, R. H.; Butts, D. M.; Ashby, D. S.; Choi, C. S.; Dunn, B. S. Sulfide Solid Electrolytes for Lithium Battery Applications. *Adv. Energy Mater.* 2018, 1800933, 1800933.
- (2) Banerjee, A.; Wang, X.; Fang, C.; Wu, E. A.; Meng, Y. S. Interfaces and Interphases in All-Solid-State Batteries with Inorganic Solid Electrolytes. *Chemical Reviews*.

 American Chemical Society July 22, 2020, pp 6878–6933.
- (3) Qiao, Y.; He, Y.; Jiang, K.; Liu, Y.; Li, X.; Jia, M.; Guo, S.; Zhou, H. High-Voltage Li-Ion Full-Cells with Ultralong Term Cycle Life at Elevated Temperature. *Adv. Energy Mater.* **2018**, *8* (33), 1802322.
- (4) Liu, X.; Li, X.; Li, H.; Wu, H. Bin. Recent Progress of Hybrid Solid-State Electrolytes for Lithium Batteries. *Chem. A Eur. J.* **2018**, *24* (69), 18293–18306.
- (5) Cai, G.; Yin, Y.; Xia, D.; Chen, A. A.; Holoubek, J.; Scharf, J.; Yang, Y.; Koh, K. H.; Li, M.; Davies, D. M.; et al. Sub-Nanometer Confinement Enables Facile Condensation of Gas Electrolyte for Low-Temperature Batteries. *Nat. Commun.* 2021 121 2021, 12 (1), 1–11.
- (6) Choi, C. S.; Whang, G. J.; McNeil, P. E.; Dunn, B. S. Photopatternable Porous Separators for Micro-Electrochemical Energy Storage Systems. *Adv. Mater.* **2022**, *34* (9).
- (7) Ashby, D. S.; DeBlock, R. H.; Lai, C. H.; Choi, C. S.; Dunn, B. S. Patternable, Solution-Processed Ionogels for Thin-Film Lithium-Ion Electrolytes. *Joule* **2017**, *1* (2), 344–358.
- (8) Delannoy, P. E.; Riou, B.; Lestriez, B.; Guyomard, D.; Brousse, T.; Le Bideau, J. Toward Fast and Cost-Effective Ink-Jet Printing of Solid Electrolyte for Lithium Microbatteries. *J. Power Sources* **2015**, *274*, 1085–1090.

- (9) Jung, J.; Won, J.; Hwang, S. S. Highly Selective Composite Membranes Using Ladder-like Structured Polysilsesquioxane for a Non-Aqueous Redox Flow Battery. *J. Memb. Sci.* 2020, 595, 117520.
- (10) Wu, P.-W.; Holm, S. R.; Duong, A. T.; Dunn, B.; Kaner, R. B. A Sol-Gel Solid Electrolyte with High Lithium Ion Conductivity. *Chem. Mater.* **1997**, *9*, 1004–1011.
- (11) Guyomard-Lack, A.; Delannoy, P.-E.; Dupré, N.; Cerclier, C. V; Humbert, B.; Le Bideau, J. Destructuring Ionic Liquids in Ionogels: Enhanced Fragility for Solid Devices. *PCCP* **2014**, *16* (43), 23639–23645.
- (12) Fromling, T.; Kunze, M.; Schonhoff, M.; Sundermeyer, J.; Roling, B. Enhanced Lithium Transference Numbers in Ionic Liquid Electrolytes. *J. Phys. Chem. B* **2008**, *112* (41), 12985–12990.
- (13) Ong, S. P.; Andreussi, O.; Wu, Y.; Marzari, N. Electrochemical Windows of Room-Temperature Ionic Liquids from Molecular Dynamics and Density Functional Theory Calculations. *Chem. Mater.* **2011**, *23*, 2979–2986.
- (14) Sharp, K. G. A Two-Component, Non-Aqueous Route to Silica Gel. *J. Sol-Gel Sci. Technol.* **1994**, *2*, 35–41.
- (15) Xu, K. Nonaqueous Liquid Electrolytes for Lithium-Based Rechargeable Batteries. *Chem. Rev.* **2004**, *104* (10), 4303–4417.
- (16) Gupta, A.; Bhargav, A.; Manthiram, A. Highly Solvating Electrolytes for Lithium—Sulfur Batteries. *Adv. Energy Mater.* **2019**, *9* (6), 1803096.
- (17) Wang, L. S.; Wang, X. X.; Li, Y.; Jiang, K.; Shao, X. Z.; Du, C. J. Ionic Liquids: Solubility Parameters and Selectivities for Organic Solutes. *AIChE J.* **2013**, *59* (8), 3034–3041.
- (18) Janz, G. J.; Ambrose, J.; Coutts, J. W.; Downey, J. R. Raman Spectrum of Propylene Carbonate. *Spectrochim. Acta Part A Mol. Spectrosc.* **1979**, *35* (2), 175–179.
- (19) Muhuri, P. K.; Das, B.; Hazra, D. K. Ionic Association of Some Lithium Salts in 1,2-Dimethoxyethane. A Raman Spectroscopic and Conductivity Study. *J. Phys. Chem. B* **1997**, *101* (17), 3329–3332.
- (20) Mohaček-Grošev, V.; Furić, K.; Ivanković, H. Observed Bands in Raman and Infrared Spectra of 1,3-Dioxolane and Their Assignments. *Vib. Spectrosc.* **2013**, *64*, 101–107.
- (21) Cheng, H.; Zhu, J.; Jin, H.; Gao, C.; Liu, H.; Cai, N.; Liu, Y.; Zhang, P.; Wang, M. In Situ Initiator-Free Gelation of Highly Concentrated Lithium Bis(Fluorosulfonyl)Imide-1,3-Dioxolane Solid Polymer Electrolyte for High Performance Lithium-Metal Batteries. *Mater. Today Energy* **2021**, *20*, 100623.

- (22) Sugiyama, J.-I.; Ueda, M.; Endo, T. Cationic Double Isomerization Polymerization of 4-Methylene-2-Phenyl-2-Styryl-l,3-Dioxolane Catalyzed by Acidic Silica Gel. *Macromolecules* **1995**, *28*, 6735–6738.
- (23) Yang, B.; Li, C.; Zhou, J.; Liu, J.; Zhang, Q. Pyrrolidinium-Based Ionic Liquid Electrolyte with Organic Additive and LiTFSI for High-Safety Lithium-Ion Batteries. *Electrochim. Acta* **2014**, *148*, 39–45.
- (24) Vogl, T.; Menne, S.; Balducci, A. Mixtures of Protic Ionic Liquids and Propylene Carbonate as Advanced Electrolytes for Lithium-Ion Batteries. *Phys. Chem. Chem. Phys.* **2014**, *16* (45), 25014–25023.
- (25) Carbone, L.; Gobet, M.; Peng, J.; Devany, M.; Scrosati, B.; Greenbaum, S.; Hassoun, J. Comparative Study of Ether-Based Electrolytes for Application in Lithium-Sulfur Battery. *ACS Appl. Mater. Interfaces* **2015**, *7* (25), 13859–13865.
- (26) Zhang, S.; Zhang, J.; Zhang, Y.; Deng, Y. Nanoconfined Ionic Liquids. *Chem. Rev.* **2016**, *117* (10), 6755–6833.
- (27) Black, J. M.; Zhu, M.; Zhang, P.; Unocic, R. R.; Guo, D.; Okatan, M. B.; Dai, S.; Cummings, P. T.; Kalinin, S. V.; Feng, G.; Balke, N. Fundamental Aspects of Electric Double Layer Force-Distance Measurements at Liquid-Solid Interfaces Using Atomic Force Microscopy. *Sci. Rep.* **2016**, *6* (1), 1–12.
- (28) Guyomard-Lack, A.; Said, B.; Dupré, N.; Galarneau, A.; Le Bideau, J. Enhancement of Lithium Transport by Controlling the Mesoporosity of Silica Monoliths Filled by Ionic Liquids. *New J. Chem.* **2016**, *40* (5), 4269–4276.
- (29) Zheng, J.; Fan, X.; Ji, G.; Wang, H.; Hou, S.; DeMella, K. C.; Raghavan, S. R.; Wang, J.; Xu, K.; Wang, C. Manipulating Electrolyte and Solid Electrolyte Interphase to Enable Safe and Efficient Li-S Batteries. *Nano Energy* 2018, 50, 431–440.
- (30) Kondo, K.; Sano, M.; Hiwara, A.; Omi, T.; Fujita, M.; Kuwae, A.; Iida, M.; Mogi, K.; Yokoyama, H. Conductivity and Solvation of Li+ Ions of LiPF6 in Propylene Carbonate Solutions. *J. Phys. Chem. B* **2000**, *104* (20), 5040–5044.
- (31) Zhao, Q.; Liu, X.; Stalin, S.; Khan, K.; Archer, L. A. Solid-State Polymer Electrolytes with in-Built Fast Interfacial Transport for Secondary Lithium Batteries. *Nat. Energy* **2019**, *4* (5), 365–373.
- (32) Nayeri, M.; Aronson, M. T.; Bernin, D.; Chmelka, B. F.; Martinelli, A. Surface Effects on the Structure and Mobility of the Ionic Liquid C6C1ImTFSI in Silica Gels. *Soft Matter* **2014**, *10* (30), 5618.
- (33) Singh, M. P.; Verma, Y. L.; Gupta, A. K.; Singh, R. K.; Chandra, S. Changes in

- Dynamical Behavior of Ionic Liquid in Silica Nano-Pores. *Ionics (Kiel)*. **2014**, *20* (4), 507–516.
- (34) Agata, Y.; Yamamoto, H. Determination of Hansen Solubility Parameters of Ionic Liquids Using Double-Sphere Type of Hansen Solubility Sphere Method. *Chem. Phys.* **2018**, *513*, 165–173.
- (35) Abbott, S.; Hansen, C. M.; Valpey, R. S. *Hansen Solubility Parameters in Practice*; Abbot, S., Hansen, C., Yamamoto, H., Eds.; Hansen-Solbility.com, 2008.
- (36) Tan, G.; Wu, F.; Zhan, C.; Wang, J.; Mu, D.; Lu, J.; Amine, K. Solid-State Li-Ion Batteries Using Fast, Stable, Glassy Nanocomposite Electrolytes for Good Safety and Long Cycle-Life. *Nano Lett.* **2016**, *16* (3), 1960–1968.
- (37) Jayakody, N. K.; Fraenza, C. C.; Greenbaum, S. G.; Ashby, D.; Dunn, B. S. NMR Relaxometry and Diffusometry Analysis of Dynamics in Ionic Liquids and Ionogels for Use in Lithium-Ion Batteries. *J. Phys. Chem. B* **2020**, *124* (31), 6843–6856.
- (38) Mestre-Aizpurua, F.; Hamelet, S.; Masquelier, C.; Palacín, M. R. High Temperature Electrochemical Performance of Nanosized LiFePO4. *J. Power Sources* **2010**, *195* (19), 6897–6901.
- (39) Plylahan, N.; Kerner, M.; Lim, D.-H.; Matic, A.; Johansson, P. Ionic Liquid and Hybrid Ionic Liquid/Organic Electrolytes for High Temperature Lithium-Ion Battery Application. *Electrochim. Acta* **2016**, *216*, 24–34.
- (40) Hess, S.; Wohlfahrt-Mehrens, M.; Wachtler, M. Flammability of Li-Ion Battery Electrolytes: Flash Point and Self-Extinguishing Time Measurements. *J. Electrochem. Soc.* **2015**, *162* (2), A3084–A3097.
- (41) Huang, J.; Hollenkamp, A. F. Thermal Behavior of Ionic Liquids Containing the FSI Anion and the Li + Cation. *J. Phys. Chem. C* **2010**, *114* (49), 21840–21847.
- (42) Thenuwara, A. C.; Shetty, P. P.; Kondekar, N.; Sandoval, S. E.; Cavallaro, K.; May, R.; Yang, C. T.; Marbella, L. E.; Qi, Y.; McDowell, M. T. Efficient Low-Temperature Cycling of Lithium Metal Anodes by Tailoring the Solid-Electrolyte Interphase. *ACS Energy Lett.* **2020**, *5* (7), 2411–2420.
- (43) Holoubek, J.; Liu, H.; Wu, Z.; Yin, Y.; Xing, X.; Cai, G.; Yu, S.; Zhou, H.; Pascal, T. A.; Chen, Z.; Liu, P. Tailoring Electrolyte Solvation for Li Metal Batteries Cycled at Ultra-Low Temperature. *Nat. Energy* **2021**, *6*, 303–313.
- (44) Fan, X.; Ji, X.; Chen, L.; Chen, J.; Deng, T.; Han, F.; Yue, J.; Piao, N.; Wang, R.; Zhou, X.; Xiao, X.; Chen, L.; Wang, C. All-Temperature Batteries Enabled by Fluorinated Electrolytes with Non-Polar Solvents. *Nat. Energy* **2019**, *4* (10), 882–890.

- (45) Damrauer, R.; Crowell, A. J.; Craig, C. F. Electron, Hydride, and Fluoride Affinities of Silicon-Containing Species: Computational Studies. *J. Am. Chem. Soc.* **2003**, *125* (35), 10759–10766.
- (46) Barrera, T. P.; Wasz, M. L. Spacecraft Li-Ion Battery Power System State-of-Practice: A Critical Review. In *2018 International Energy Conversion Engineering Conference*; 2018; p 4495.
- (47) Brinker, C. J. Hydrolysis and Condensation of Silicates. *J. Non. Cryst. Solids* **1988**, *100*, 31–50.
- (48) Ashby, D. S.; Choi, C. S.; Edwards, M. A.; Talin, A. A.; White, H. S.; Dunn, B. S. High-Performance Solid-State Lithium-Ion Battery with Mixed 2D and 3D Electrodes. *ACS Appl. Energy Mater.* **2020**, *3* (9), 8402–8409.
- (49) Aegerter, M. A.; Prassas, M. *Aerogels Handbook*; Aegerter, M. A., Leventis, N., Koebel, M., Eds.; Springer, 2011.
- (50) Ashby, D. S.; Deblock, R. H.; Choi, C. S.; Sugimoto, W.; Dunn, B. Electrochemical and Spectroscopic Analysis of the Ionogel-Electrode Interface. *ACS Appl. Mater. Interfaces* **2019**, *11* (12), 12088–12097.
- (51) Rivnay, J.; Inal, S.; Salleo, A.; Owens, R. M.; Berggren, M.; Malliaras, G. G. Organic Electrochemical Transistors. *Nature Reviews Materials*. Nature Publishing Group January 16, 2018, pp 1–14.
- (52) Deblock, R. H.; Wei, Q.; Ashby, D. S.; Butts, D. M.; Whang, G. J.; Choi, C. S.; Dunn, B. S. Siloxane-Modified, Silica-Based Ionogel as a Pseudosolid Electrolyte for Sodium-Ion Batteries. ACS Appl. Energy Mater. 2021, 4 (1), 154–163.
- (53) Mistry, A.; Fear, C.; Carter, R.; Love, C. T.; Mukherjee, P. P. Electrolyte Confinement Alters Lithium Electrodeposition. *ACS Energy Lett.* **2019**, *4* (1), 156–162.
- (54) Gurikov, P.; S. P., R.; Griffin, J. S.; Steiner, S. A.; Smirnova, I. Solvent Exchange in the Processing of Biopolymer Aerogels: Current Status and Open Questions. *Ind. Eng. Chem. Res.* **2019**, *58* (40), 18590–18600.

Supporting Information

Modifying Ionogel Solid-Electrolytes for Complex Electrochemical Systems

 $David\ S\ Ashby^{l,\,*},\ Jorge\ Cardenas^2,\ Austin\ Suhas\ Bhandarkar^l,\ Adam\ W.\ Cook^2,\ \&\ A.\ Alection Talin^{l,\,*}$

¹Sandia National Laboratories, Livermore, California 94550, USA

²Sandia National Laboratories, Albuquerque, New Mexico 87123, USA

*Corresponding Authors: dsashby18@gmail.com, aatalin@sandia.gov

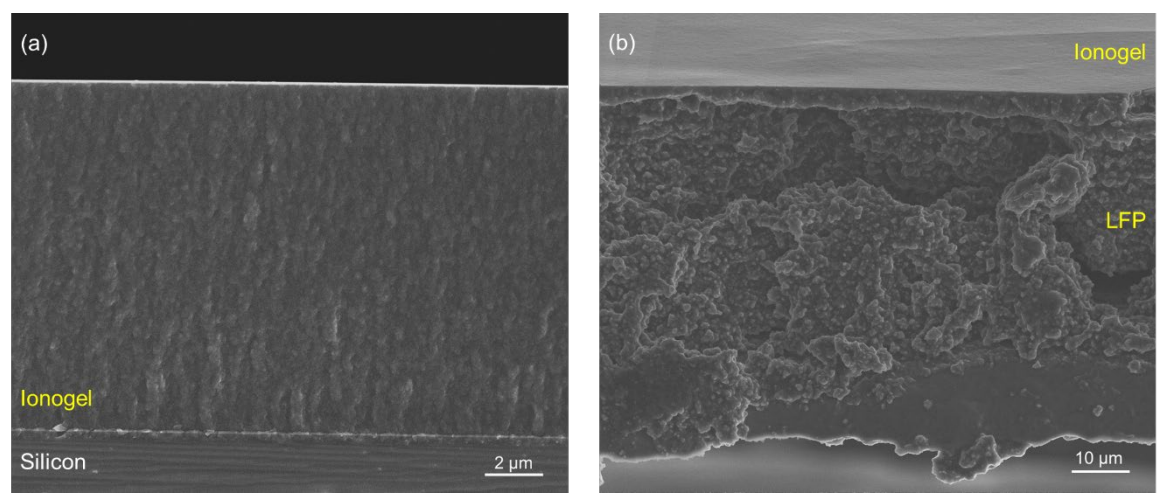


Figure S1. Spun Ionogel Films

a) SEM cross-sectional of a spin-coated ionogel on a silicon wafer. The film is approximately 10 microns in thickness. The corresponding regions are labeled. b) SEM image of an ionogel spun onto a cast LFP electrode using the same conditions as (a).

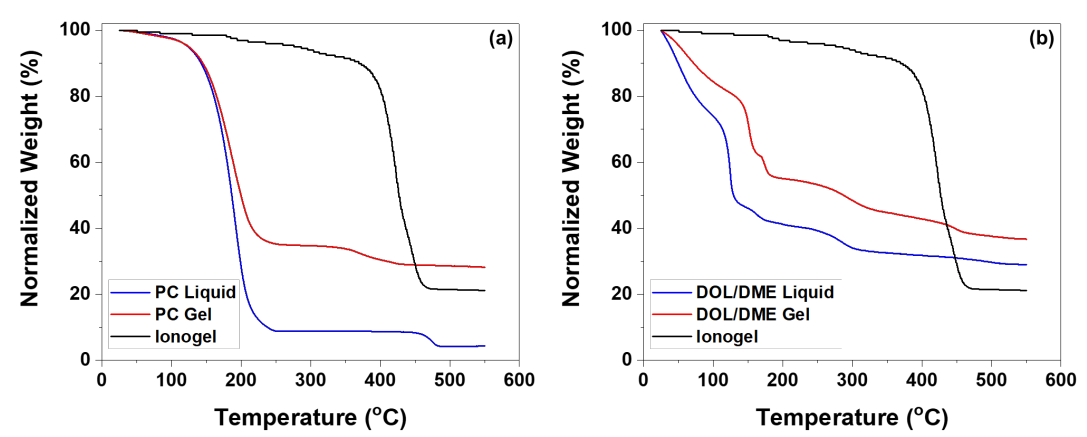


Figure S2. Thermal Gravimetric Analysis of Solvent-Exchanged Gels a) TGA analysis of a PC gel (red) compared to an ionogel (blue) and neat liquid (black). b) TGA analysis of a DOL/DME gel (red) compared to an ionogel (blue) and neat liquid (black). There is no indication of ionic liquid (~400 °C) still trapped inside the matrix after solvent exchange. The loss at ~350 °C corresponds to loss of vinyl groups in the matrix. A shift in the decomposition temperature is identified after entrapment inside the gel, as expected from nanoconfinement. The residual weight at 600 °C, associated with residual silica, falls within the range expected for this silica-gel synthesis process.

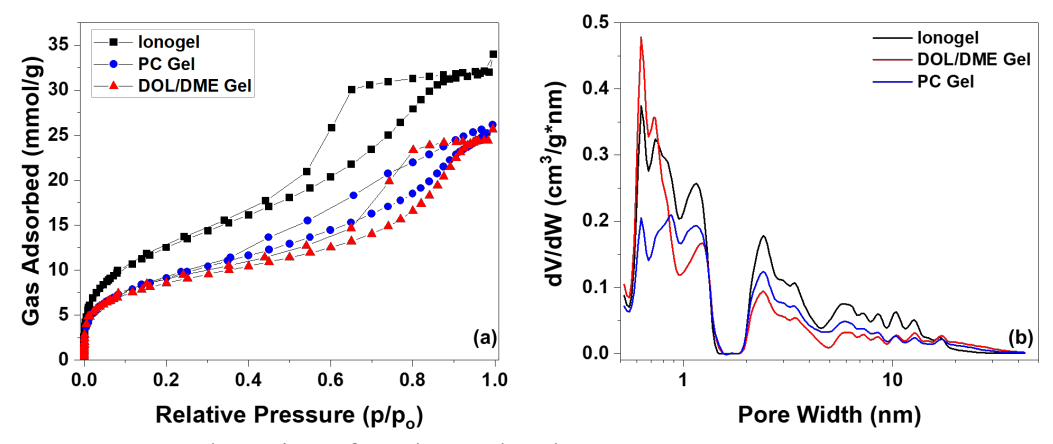


Figure S3. Gas Adsorption of Exchanged Gels a) N₂ adsorption isotherm for a super-critically dried ionogel (black), PC-exchanged gel (blue), and DOL/DME-exchanged gel (red). a) Pore size distribution for a super-critically dried ionogel (black), PC-exchanged gel (blue), and DOL/DME-exchanged gel (red). While a decrease in the available surface for gas adsorption is identified after solvent exchange, the gels still maintain a high surface area of over 700 m² g⁻¹. The loss could be attributed to pore collapse during drying from incomplete exchange with CO₂ or the intermediate alcohol solvent. The pore distribution indicates no rearrangement of the silica moieties occur during exchange, with the distribution determined by the original ionic liquid molecular size and stacking.

S-4

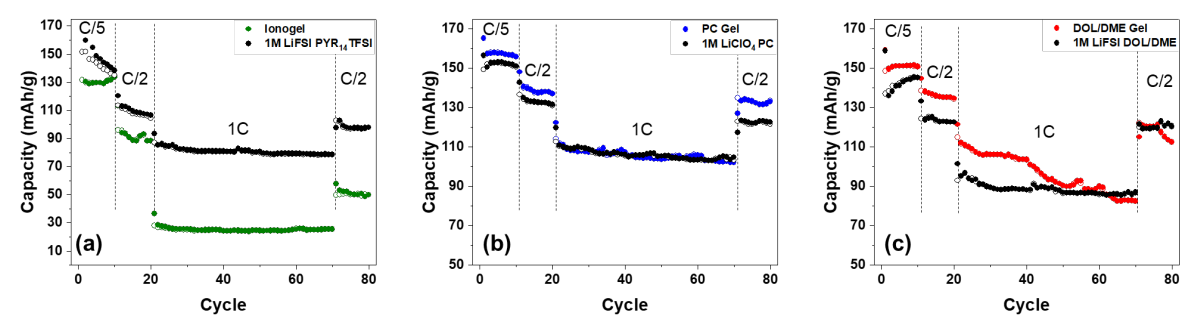


Figure S4. Electrochemical Comparison of Gel vs. Liquid Electrolytes Capacity variation comparison with cycling at varying C rates for the ionic-liquid-based systems (a) PC based systems (b) and DOL/DME systems (c).

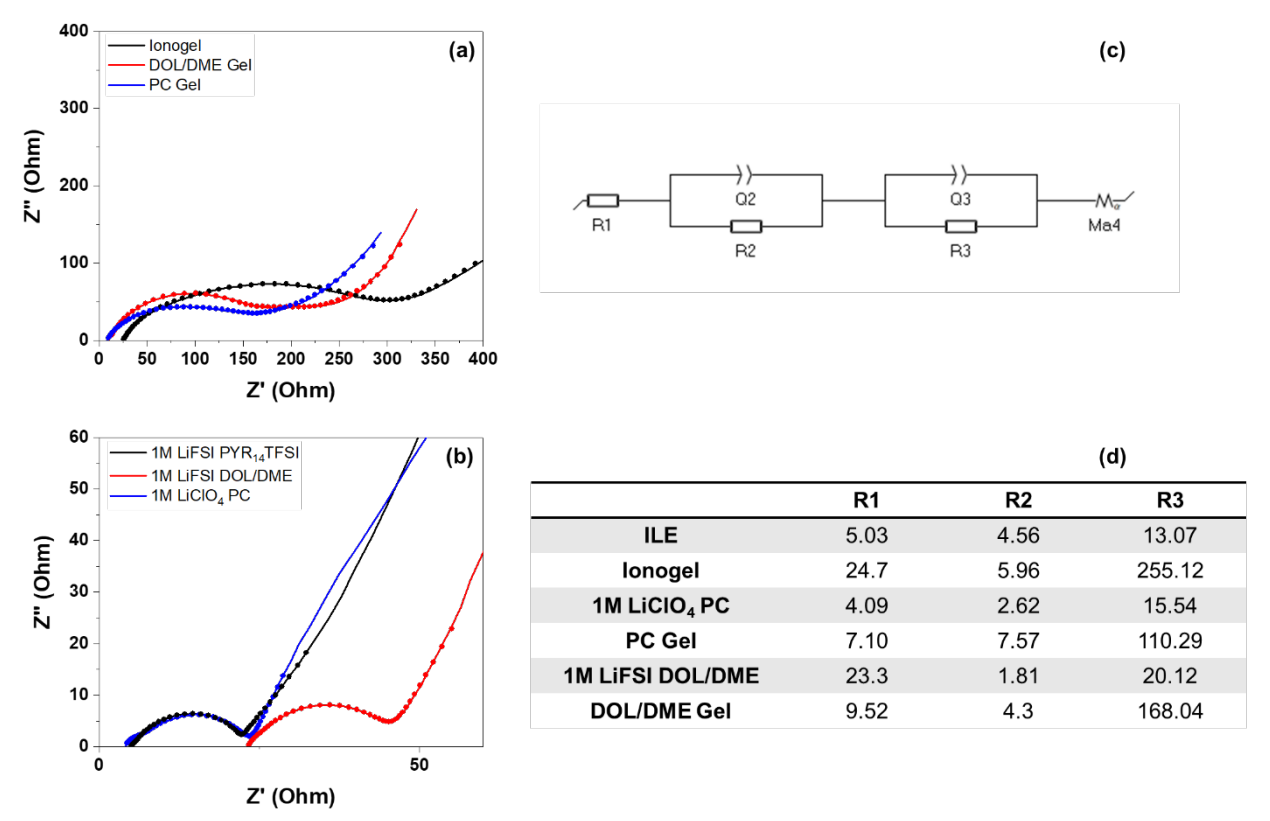


Figure S5. EIS Analysis of Solvent-Exchanged Gels

a) EIS before cycling of LFP/Li cells containing ionogel (black), DOL/DME (red), or PC (blue) gels. b) EIS before cycling of LFP/Li cells containing ILE (black), DOL/DME (red), or PC (blue) liquid electrolyte. Experimental data consist of the lines while the fits correspond to the circles. c) Corresponding circuit used for fitting the EIS data. d) Fitting resistances for the series, gel, and charge transfer resistances, respectively, for the corresponding circuit (c). While we see that all three electrolytes have similar charge transfer resistances, exchanging the ILE with PC significantly reduces the resistance of the gel. The decrease in gel resistance corresponds well the rate capability of the different cells (**Figure 2**), with the PC system performing the best and ionogel showing the worst performance. The increase in the LFP charge transfer resistance after addition of the gel likely originates from LiCO₃ species that form on the surface from the acidity of the sol. While there is an increase, it is not significant enough to affect the electrochemical performance of the PC-exchanged gel.

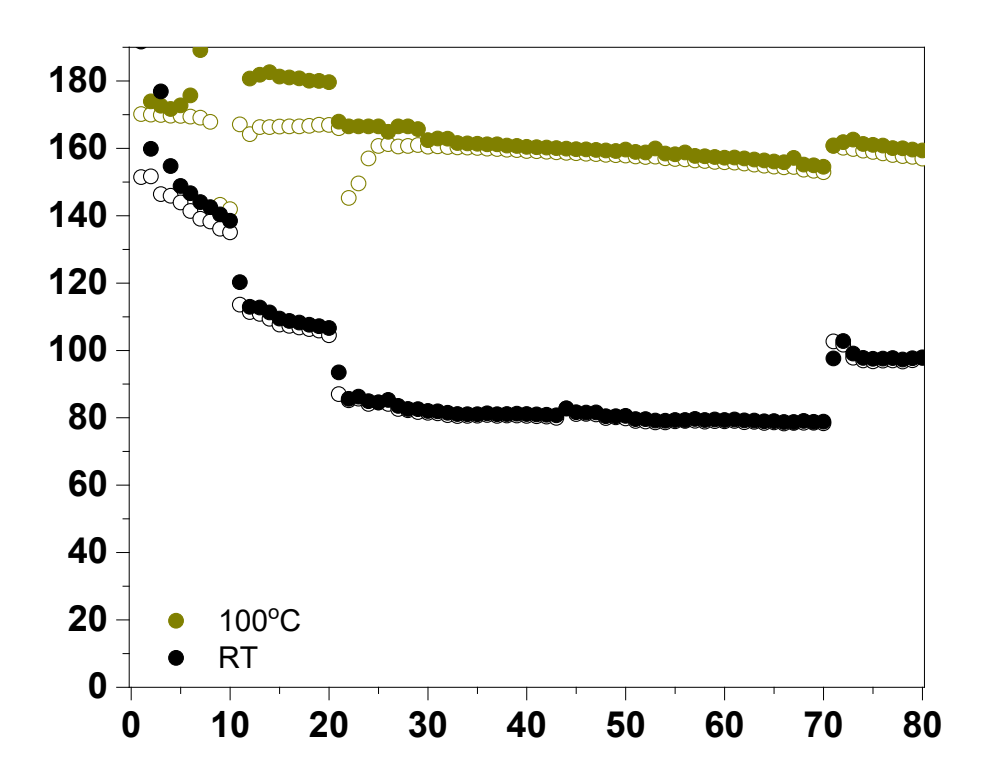


Figure S6. Electrochemical Performance for an ILE Cell at Various Temperatures Electrochemical performance for a LFP/ILE/Li metal cell at room temperature (green) and 100 °C (gold). A significant cycling inefficiency is identified for the neat ionic liquid system, in comparison to ionogels (**Figure 3**), that becomes more substantial as the temperature is raised. This instability is likely due to side reactions with the Li metal that are suppressed when using the ionogel or by going to higher rates.

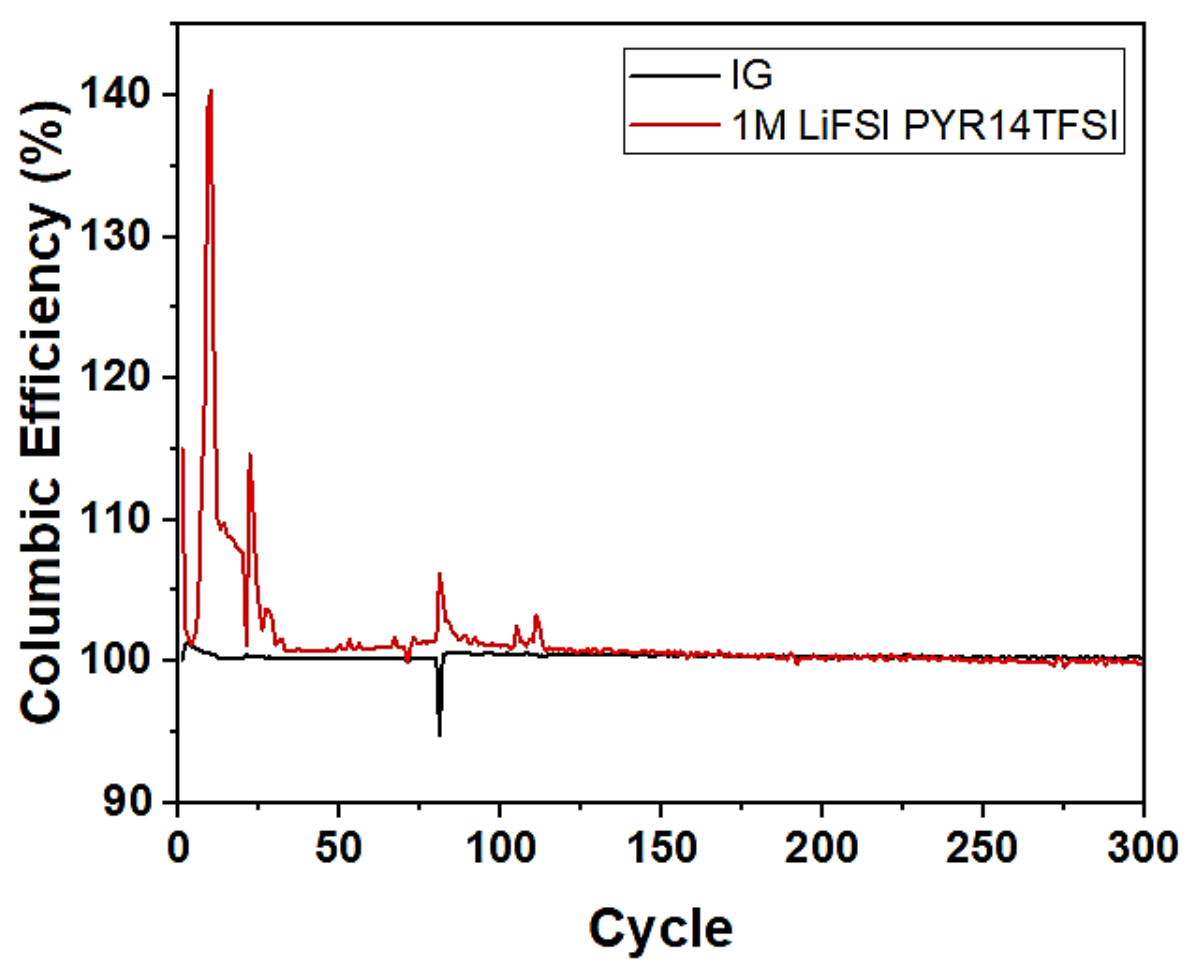


Figure S7: Columbic Efficiency vs Cycle for 100°C Cycling

Columbic efficiency for the cycling of the ionic liquid and ionogel systems at 100°C shown in figure 3b and S5. An improved stability is found by using an ionogel over the base liquid, likely from stabalizing the SEI formed on the interface of the Li anode.

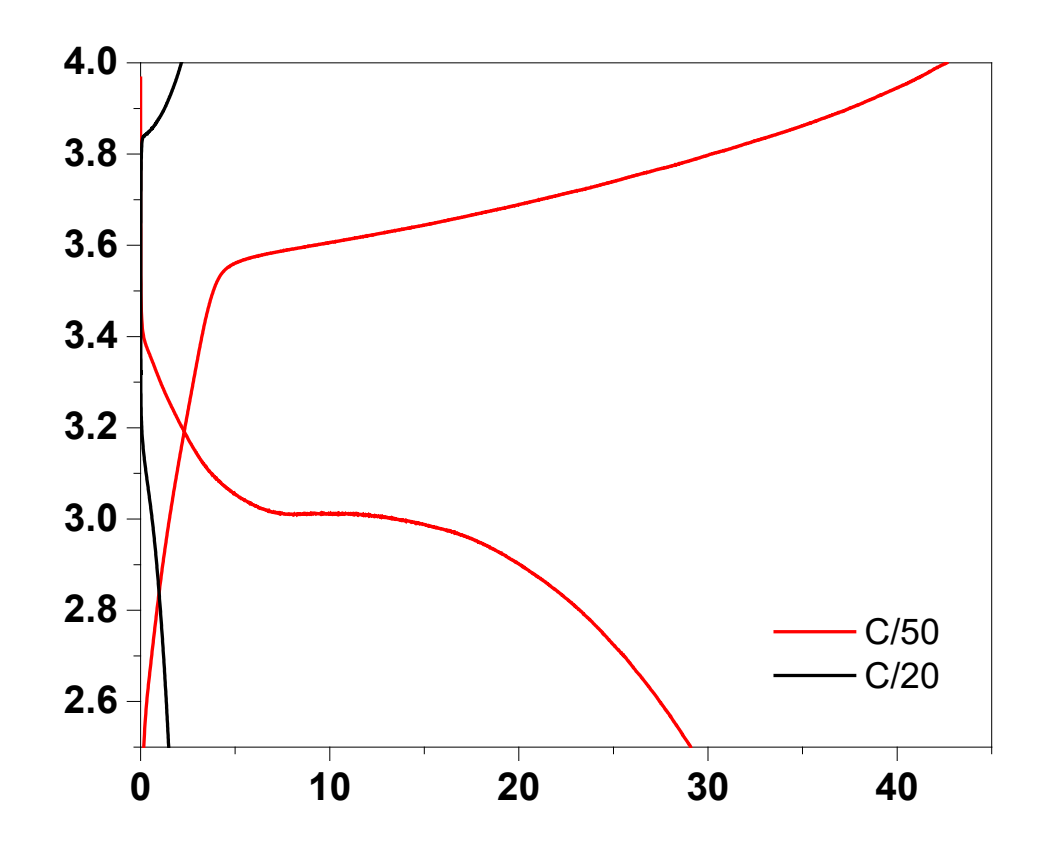


Figure S8. Low Temperature Performance of an Ionogel Cell Galvanostatic cycles at C/50 and C/20 for a LFP/ionogel/Li metal cell at -40 °C. While the ionogel shows adequate conductivity at -40 °C (~0.5 mS cm⁻¹, **Figure 1c**), when it is incorporated into the cell a significant polarization is found that significantly decreases the achievable capacity, even at very low currents. It is unclear whether this decreased capacity is related to freezing of the ILE, or inefficiency of charge transfer at the Li or LFP interface.

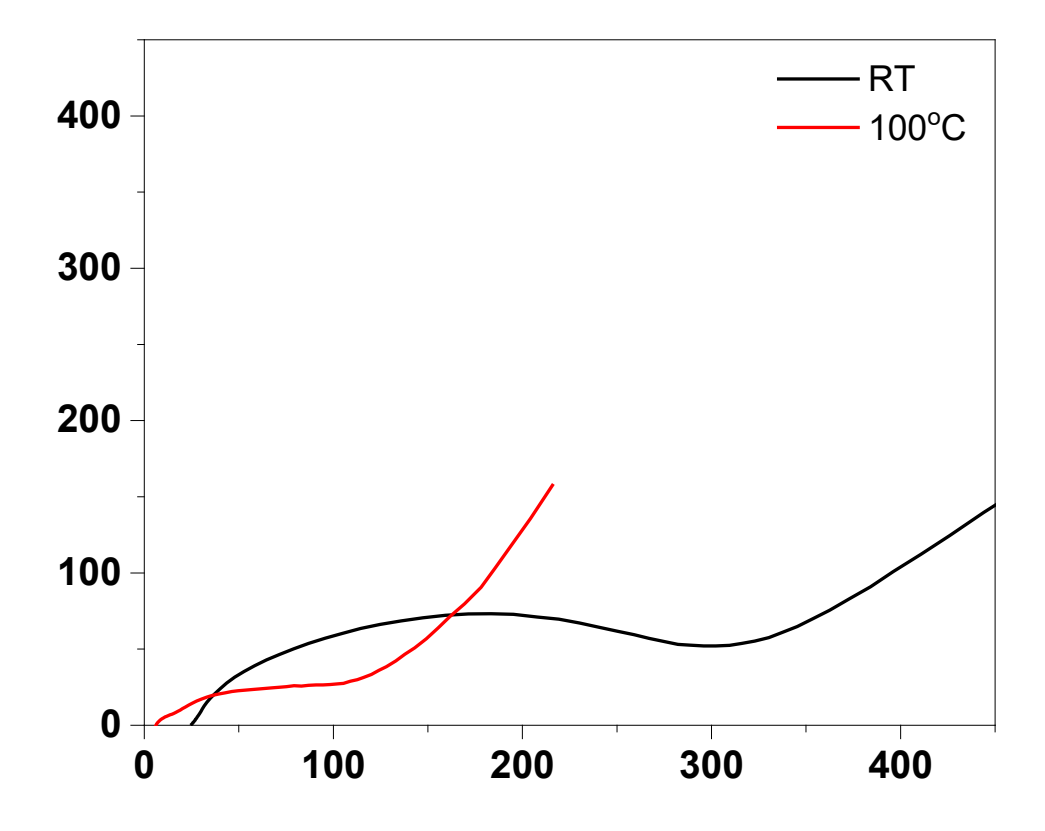


Figure S9. EIS of Ionogel with Temperature EIS before cycling LFP/Li cells containing ionogel at room temperature (black) and 100 °C (red). A significant decrease in the electrolyte resistance and charge transfer resistance is identified for the high temperature system, correlating to the improved electrochemical performance (**Figure 3b**).

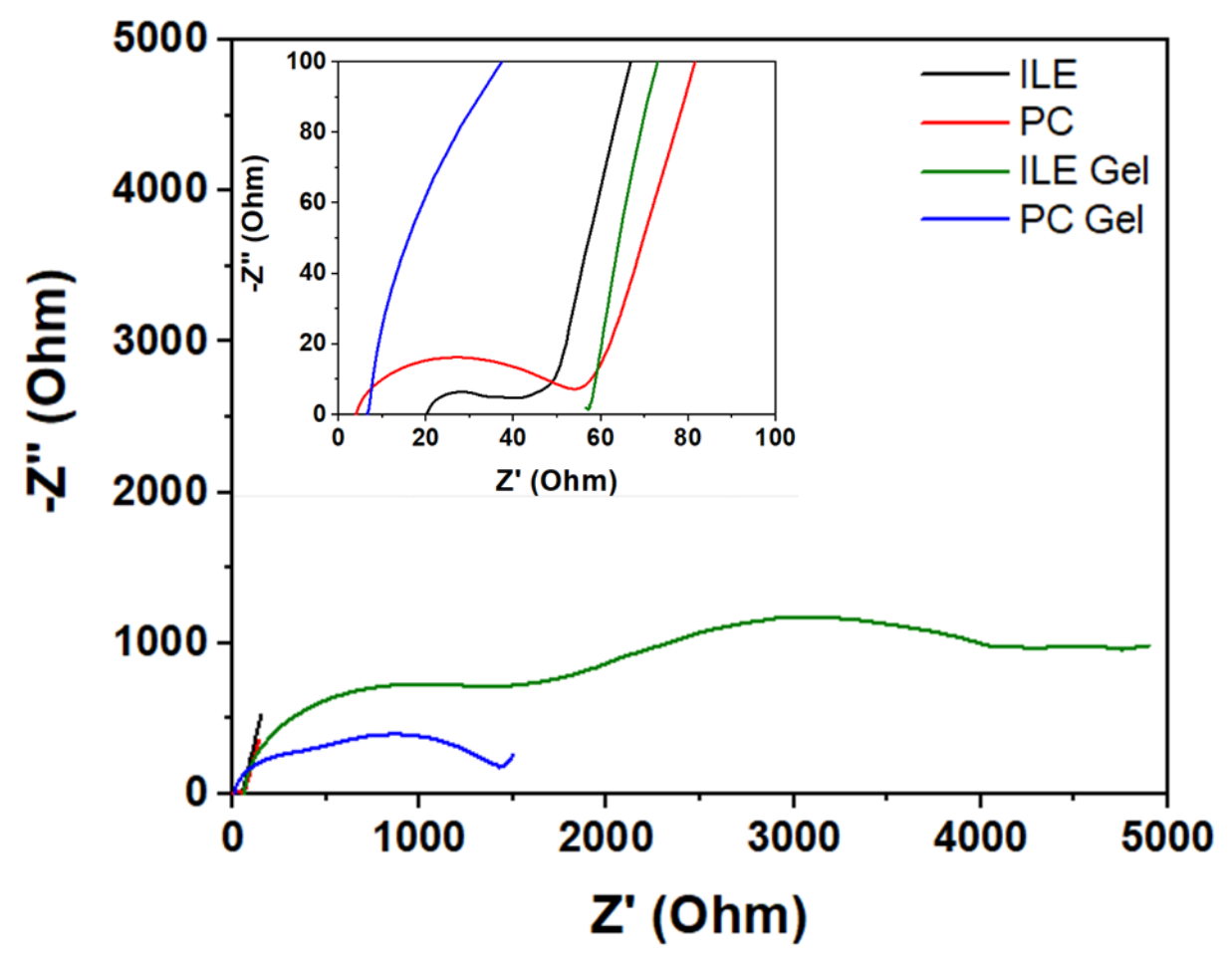


Figure S10. EIS of the AM LFP/LTO Cells with Various Electrolytes Electrochemical impedance spectroscopy of the cells cycled in **Figure 4b**. The inset of the low resistance region is included. Significantly lower impedances occurred after exchanging the PC electrolyte for the ILE in the gels though they are still notably higher than the base liquids.



Video S1. ILE Gel Printing Process

Exemplary video of ionogel printing process onto a standard substrate. The printing process can be found outline in the methods.